Analysis and adaptive mitigation scheme of low-frequency oscillations in railway traction power systems

Jiang, Xiaofeng; Hu, Haitao; Yang, Xiaowei; He, Zhengyou; Qian, Qingquan; Tricoli, Pietro

DOI:
10.1109/TTE.2019.2927128

License:
Other (please specify with Rights Statement)

Document Version
Peer reviewed version

Citation for published version (Harvard):
Jiang, X, Hu, H, Yang, X, He, Z, Qian, Q & Tricoli, P 2019, 'Analysis and adaptive mitigation scheme of low-frequency oscillations in railway traction power systems', *IEEE Transactions on Transportation Electrification*. https://doi.org/10.1109/TTE.2019.2927128

Analysis and Adaptive Mitigation Scheme of Low-Frequency Oscillations in Railway Traction Power Systems

Xiaofeng Jiang, Haitao Hu, *Member, IEEE*, Xiaowei Yang, Zhengyou He, *Senior Member, IEEE*, Qingquan Qian, and Pietro Tricoli, *Member, IEEE*

The authors: Xiaofeng Jiang, Haitao Hu, Xiaowei Yang, Zhengyou He, and Qingquan Qian are with the College of Electrical Engineering, Southwest Jiaotong University, Chengdu 611756, China. (e-mail: jxf@my.swjtu.edu.cn, hht@swjtu.edu.cn, yxwswjtu@163.com, hezy@swjtu.edu.cn, qqq@swjtu.edu.cn); Pietro Tricoli is with the Department of Electronic, Electrical and Systems Engineering, University of Birmingham, Birmingham B15 2TT, U.K. (e-mail:p.tricoli@bham.ac.uk).

The corresponding author is Zhengyou He. Currently, he is a Professor at Southwest Jiaotong University, Chengdu 611756, China. TEL: +86 13908066782. E-mail: hezy@swjtu.edu.cn.

This paper is not presented at any prior presentation and publication at a conference or prior submission to any other publication.

Abstract—The diffusion of modern electric trains equipped with high-power voltage-source converters has introduced new dynamic interactions with the traction power system that may create unexpected low-frequency oscillations . This paper presents for the first time a detailed analysis of the operating condition of electric trains and traction network, revealing that specific changes of the operating conditions of the train-network system are responsible for the oscillations and may lead to instability. The study is carried out with an analytical dynamic model considering the transient direct current control and focusses on understanding how the mismatch between the actual parameters of the train-network syste and those used by the controller affects system dynamic and stability. It is shown that the retuning of controller parameters improves the dynamic performance of the train-network system, and hence an adaptive control is proposed to mitigate low frequency oscillations with minimal change and cost to the original system. Simulation and experimental results are presented in the paper to fully validate the proposed control method.

Index Terms—Train-network System, Low-frequency Oscillation, Power mismatch, Parameters Tuning, Adaptive Mitigation.

I. INTRODUCTION

In recent years, AC electric trains, especially high-speed and high-power trains, have been widely adopted around the world. However, with the power increase of modern trains, stability issues have arisen at the point of connection of trains to the traction network system [1, 2]. Specially, low-frequency oscillations (LFO) of train-network system have been reported in several countries [3, 4]. LFO are distortions of the line voltage, current and DC-link voltage of the traction inverters characterized by a low-frequency fluctuation of the amplitude of these quantities and they have n adverse impact on the normal transport operations and the safety of electric railways.

A. LFO reported in electric railways

Originally, LFO was firstly reported in Europe [3], and especially in Switzerland (oscillation frequency at 5 Hzwith a fundamental frequency of the traction power supply system of 16.67 Hz) and Norway (oscillation frequency at 1.6 Hz with a fundamental frequency of the traction power supply system of 16.67 Hz) [5, 6], which resulted from the interaction between trains and the rotary frequency converters feeding the traction network. Several other cases of LFO have been detected since around the world [3, 4, 7] in parallel to the widespread diffusion of modern trains with switched-mode power converters, as indicated in Table I. Similar phenomena have occurred more frequently in China over the last decade, even if the traction power supply system only uses transformers, and LPO have caused tripping of protections and startup failure of the trains.

Table I Historical records of LFO in electric railways around the world [3-7], note that f_s is the fundamental frequency and f_l is the oscillation frequency.

No.	f_l / Hz	f_s / Hz	Site	Time
1	5	16.67	Zurich, Switzerland	1995
2	1.6	16.67	Jernbaneverket Test, Norway	1996
3	3	25	Washington, USA	2004
4	7	50	Siemens Test, Germany	2005
5	5	50	Thionville, France	2008
6	2~4	50	Hudong, China	2008
7	5	50	Shanghai, China	2010
8	5	50	Qingdao, China	2010
9	6~7	50	Shanhaiguan, China	2011
10	0.6~2	50	Xuzhou, China	2015

B. Literature review

The first studies on LFO have used simplified time-domain and enhanced RMS models of a single-phase power converter and are largely based on a linear analysis [5]. Subsequently, a small-signal model in the synchronous dq reference frame has been proposed for the train-network system for the China Railways High-speed (CRH) [8]. Based on the transfer function of the train-network system [9], derived from the relation between the trains and the traction power system, the frequency domain analysis is carried out for the main factors of LFO. Then, the impedance-based method [10, 11] is introduced to suit for the trains-network system. The impedance model of the traction network and trains in static reference frame is deduced respectively in [7]. As to the single-phase characteristic of the

traction power system and the dq decoupling vector control of the traction converter, [12] focuses on the dq-frame impedance modeling and proposes an impedance modeling method that takes into account the phase locked loop. Then, a dq-frame impedance measurement method for single-phase system based on Hilbert transform is also summarized, which provide a new verification approach for the impedance modelling.

The previous models of the train-network system and stability analysis have been specifically focused on LFO of electrified railways, but they only refer to trains with dq control. Little attention has been devoted to far to trains with transient direct current control that also cause this kind of oscillations.

The mismatch between the parameters of the traction power system and the train control system has been briefly mentioned in [9, 13], but there is no in-depth understanding of the reasons behind the oscillations. Although some papers analyze in detail the control system design and control strategy of single-phase four-quadrant pulse-width modulation (PWM) converters [14, 15] and mention specific power circuits and required control characteristics in rated conditions, only few papers attempt to understand the origin of LFO when power circuits and control systems are considered simultaneously. A mathematical model for the single-phase four-quadrant PWM converter is derived in [14] from the averaged state-space equations. From this model, a stability analysis method that includes the current control of the converter has been implemented in [16]. However, the existing controller design of the converter takes into account only the rated conditions at steady-state and a sudden change of the load, without details on the behavior for low load conditions and when multiple converters are connected simultaneously on the traction power supply. A typical occurrence of this is when the auxiliary system is powered directly from the DC-link of the main traction drive system and shares the same traction rectifiers).

The solutions in terms of LFO mitigation can be categorized into mitigation methods looking at the power supply system side, and methods looking at the train side [7]. For the the power supply side, [13, 17] propose either the installation of voltage stabilizers in the substations or the capacity upgrade of traction transformers . Other works propose the use of active compensators added in substations in a way similar to the methods used to suppress LFO in power systems [18].For the train side, [13] mainly considers the influence on stability of train number and control. It has been found that a reduced number of trains simultaneously connected to the catenary reduces the severity of LFO, but results in losing capacity and flexibility of the transport system and, thus, it can be used only as a temporary emergency plan. Another approach is based on a modification of the operating mode of PWM converters by disabling the switching and, hence,effectively using these converters as diode rectifiers [19]. Besides, [8] presents an additional power oscillation damping module in the converter control system, but the complex load characteristic leads difficulties in the practical implementation. Other control techniques, such as the multivariable control [6], the auto-disturbance rejection control [20] and the passivity-based control [21] have also tried to improve the performance of conventional control with moderate success and sometimes induce new problems.

As all the previous proposals require substantial investments on the system infrastructure and thorough control design it is necessary to introduce new mitigation methods based on the smallest possible changes to the original train-network system and control strategy.

C. Original Contributions and Organization of the paper

This paper presents a comprehensive analysis of the stability of the train-network interconnected system for operating conditions different from the rated ones. LFO are analyzed by a new small-signal model of the train-network system adopting transient direct current control that takes into account simultaneously multiple trains and light load conditions for the case of shared converters. The small-signal model is used to investigate the causes and the dynamic effects of LFO for real operating conditions and clearly reveals the mismatch between the actual controller and control objectives, which is a plausible theoretical explanation of LFO in electric railways. Moreover, the stability and dynamic performance analysis with Bode and eigenvalue plots are undertaken to explore the effects of control parameters. This allows a better understanding of the laws for tuning the controllers and developing a practical way of mitigating LFO. Finall a new adaptive mitigation scheme with minimal impact to the original systems is proposed to adaptively select the suitable parameters of the controller according to the actual load power.

The remainder of the paper is organized as follows. Section II presents the field measurement results to identify the common characteristics of LFO and indicates the requirements for the system analysis. Then, the small-signal modeling procedure of the trains-network system is formulated in detail in Section III. This is followed by the system stability and dynamic performance analysis with actual working conditions in Section IV, where the influence of different working conditions is investigated and the mismatching mechanism is presented. Section V discusses the tuning of the controller parameters and proposes the adaptive mitigation on LFO, which are verified by simulations and experiments. Finally, the conclusions are drawn in Section VI.

II. FIELD MEASUREMENTS AND COMMON CHARACTERISTICS OF LFO

Field tests have been organized to reproduce LFP on a real electric railway in China, where Fig. 1show the line voltage, line current and DC-link voltage for normal conditions (a) and presence of LFO (b). According to the tests and the related reports [22-24], the common characteristics of LFO can be summarized as follows:

(1) The envelopes of the line voltage, current and DC-link voltage show a low-frequency fluctuation at 0.6-7 Hz with constant amplitude and frequency;

(2) LFO usually occur for special loading conditions of the train-network system. In this railway, LFO occur when multiple trains are parked in the depot connected to the traction network, and draw power only for auxiliary loads.

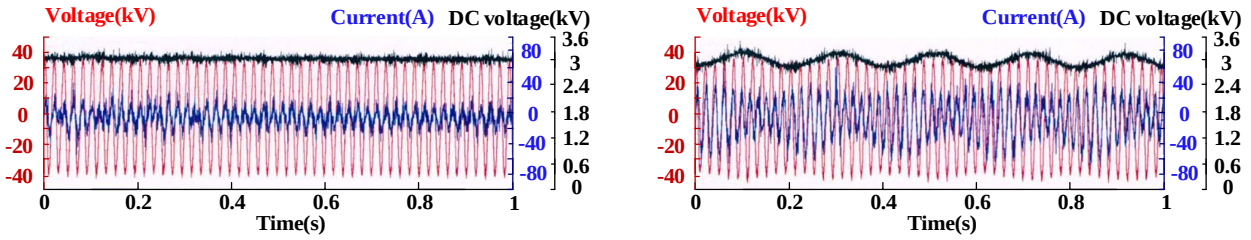

Fig.1 Line voltage, current and DC-link voltage for normal operations (a) and during LFO (b) occurring in the Chinese electric railway.

(3) The presence of LFO is related to the number of trains. The magnitude of the fluctuation gradually increases with the number of trains and becomes visible when there are at least 5~8 trains;

(4) Such oscillations cause tripping of protection and disconnection of the trains, with substantial delays to check for any anomalies of the traction system;

(5) The converters of the trains causing LFO are controlled by the transient direct current control or the dq decoupling control;

(6) In the trains causing LFO, the auxiliary system draws power directly from the DC-link through the main traction rectifier as shown in Fig. 2(a). No issues are caused by trains using independent converter for the auxiliary loads, as shown in Fig. 2(b).

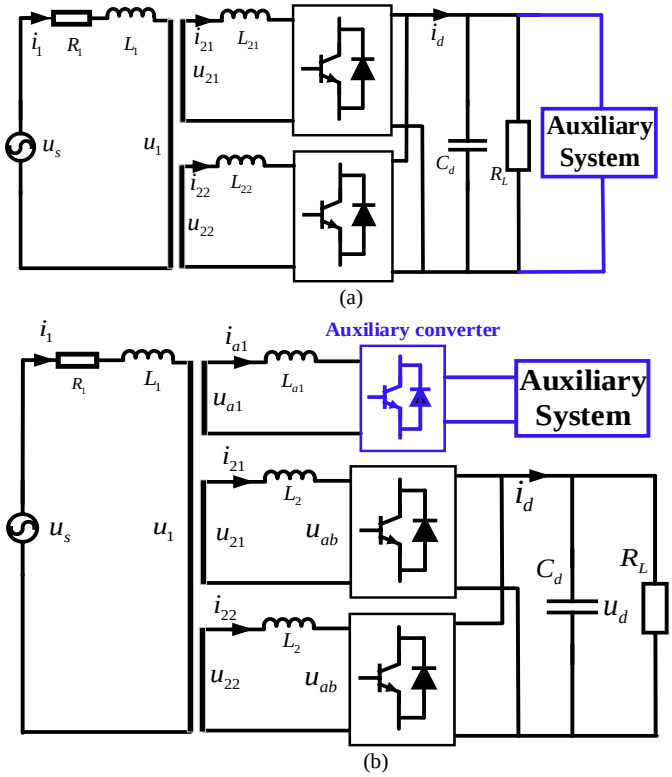

Fig.2 Circuit topology of the main traction system of locomotives or EMUs operating in the Chines electric railway. Shared rectifier for the auxiliary system and the main traction drive system (a); independent rectifier for the auxiliary system (b).

The field tests also reveal that during LFO the direction of the power changes periodically, thus the outer voltage loop and the inner current loop of the traction converter fail to reach the desired references. The origin of LFO can be attributed to the fact that the controller is designed for rated operating conditions, while the converter actually operates at low load. The characteristics of the on-site measurements can be used to develop a suitable small-signal model to interpret the presence of such oscillations and understand

how system stability is affected.

III. System Modelling

A. Assumptions and equivalent circuit

The train-network system is represented in Fig. 3 and contains the utility power system, the traction substation, the traction network and the trains parked at the depot.

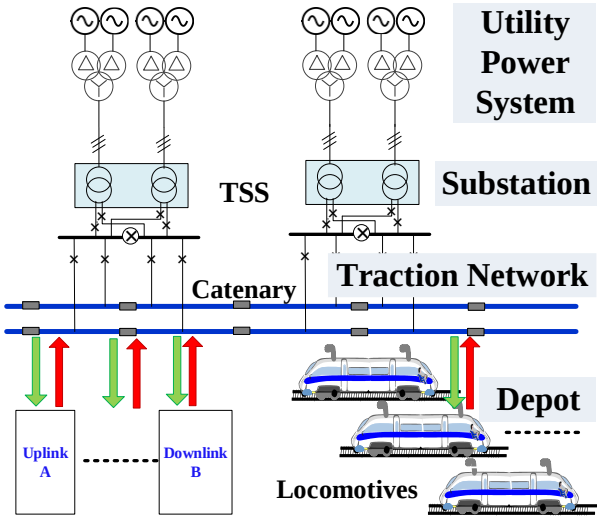

Fig.3 Structure of the train-network system.

It is assumed that the currents of all the n trains simultaneously connected to the catenary are synchronous, so that the voltage drop across the equivalent impedance of the power supply side, ΔU, is n times that of one train [25]. This is also equivalent to assume that the equivalent impedance of the power supply is n times greater than the real one, as shown in (1):

$$\Delta U = Z_s \cdot (nI) = (nZ_s) \cdot I \tag{1}$$

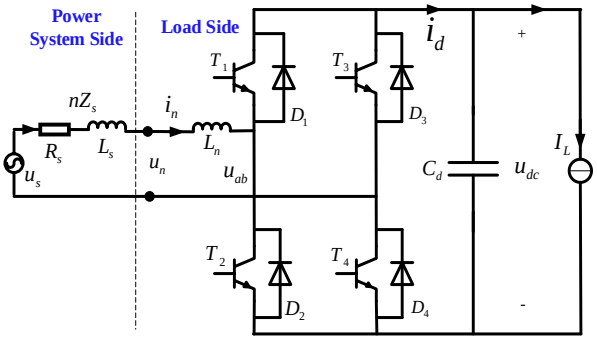

Fig.4 Equivalent circuit of train-network system referred to the secondary side of the traction transformer

The equivalent circuit of the train-network system is shown in Fig.4. In this figure, the equivalent voltage source, u_s, is the voltage of the traction power network referred to the secondary winding of the on-board transformer and, hence, it is $u_s=u_1/k$, where u_1 is the voltage of the traction power network and k is the turns ratio of the transformer; Z_s is the equivalent impedance of the traction power network referred to the secondary of the transformer, L_n is the coupling inductance of the converter, C_d is the dc-link capacitance, and I_L is the current drawn by the load that includes the traction load and the auxiliary system.

B. Small-signal model of equivalent system

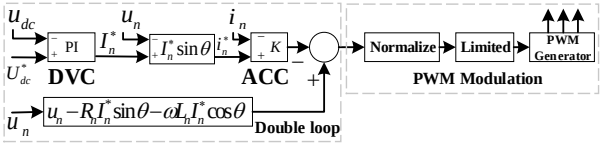

Fig.5 Block diagram of the transient direct current control

The single-phase four-quadrant converters (4QCs) use the transient direct current control as shown in Fig. 5 [26], where DVC denotes the controller of the outer voltage loop and ACC is the controller of the inner current loop. As the 4QCs are two-level converters [27], four different circuit configurations are obtained on the basis of the switches' status. Therefore, the state-space equations of the model are:

$$\begin{cases} L\dfrac{di_n}{dt} + R_s i_n + \gamma u_{dc} = u_s \\ \gamma i_n = C_d \dfrac{du_{dc}}{dt} + I_L \end{cases} \tag{2}$$

where $L=L_s+L_n$ and γ can be equal to 1, 0, or -1 depending on the switches' status. According to PWM modulation rules, γ can be expressed as a time-varying function, $\gamma = m\sin(\omega t - \lambda)$, where m denotes the modulation index and λ is the load phase angle [14, 16, 28]. Therefore, assuming a sinusoidal modulated current $i_n=i\sin\omega t$, (2) can be rearranged as:

$$\begin{cases} L\dfrac{di_n}{dt} + R_s i_n + m\sin(\omega t - \lambda)u_{dc} = u_s \\ m\sin(\omega t - \lambda) i_n = C_d \dfrac{du_{dc}}{dt} + I_L \\ u_s = U_s \sin(\omega t + \varphi) \\ i_n = i\sin\omega t \end{cases} \tag{3}$$

where φ is the power-factor angle.

Substituting the last equation into the first equation of (3) and equating separately the sine and cosine terms, it is:

$$\begin{cases} L\dfrac{di}{dt} + R_s i = -mu_{dc}\cos\lambda + U_s\cos\varphi \\ iL\omega = mu_{dc}\sin\lambda + U_s\sin\varphi \end{cases} \tag{4}$$

Furthermore, according to the second equation of (3), it is:

$$C_d\frac{du_{dc}}{dt} = \frac{1}{2}mi\cos\lambda - I_L \tag{5}$$

Therefore, the system can be represented by the following equations:

$$\begin{cases} L\dfrac{di}{dt} + R_s i = -mu_{dc}\cos\lambda + U_s\cos\varphi \\ iL\omega = mu_{dc}\sin\lambda + U_s\sin\varphi \\ C_d\dfrac{du_{dc}}{dt} = \dfrac{1}{2}mi\cos\lambda - I_L \end{cases} \tag{6}$$

These equations can then be linearized around the steady-state operating point. Indicating with capital letters the steady-state point and with $\triangle$ the deviation from the steady-state value, we have:

$$\begin{cases} m = M + \Delta m \\ u_{dc} = U_{dc} + \Delta u_{dc} \\ i = I + \Delta i \\ \lambda = \Lambda + \Delta\lambda \\ \varphi = \Phi + \Delta\varphi \end{cases} \tag{7}$$

And substituting (7) into (6), we have:

$$\begin{cases} L\dfrac{d(I+\Delta i)}{dt}+R_s(I+\Delta i)= \\ \quad -(M+\Delta m)(U_{dc}+\Delta u_{dc})\cos(\Lambda+\Delta\lambda)+U_s\cos(\Phi+\Delta\varphi) \\ (I+\Delta i)L\omega= \\ \quad (M+\Delta m)(U_{dc}+\Delta u_{dc})\sin(\Lambda+\Delta\lambda)+U_s\sin(\Phi+\Delta\varphi) \\ C_d\dfrac{d(U_{dc}+\Delta u_{dc})}{dt}= \\ \quad \dfrac{1}{2}(M+\Delta m)(I+\Delta i)\cos(\Lambda+\Delta\lambda)-I_L \end{cases} \tag{8}$$

Using the first-order approximations of the Taylor Series for the sine and cosine terms:

$$\begin{cases} \sin(X+\Delta x)\approx \sin X+\Delta x\cos X \\ \cos(X+\Delta x)\approx \cos X-\Delta x\sin X \end{cases} \tag{9}$$

and applying (9) to (8), the steady-state terms of the model are:

$$\begin{cases} R_s I=-MU_{dc}\cos\Lambda+U_s\cos\Phi \\ IL\omega=MU_{dc}\sin\Lambda+U_s\sin\Phi \\ 0=\dfrac{1}{2}MI\cos\Lambda-I_L \end{cases} \tag{10}$$

whereas the small-signal model is given by:

$$\begin{cases} L\dfrac{d\Delta i}{dt}+R_s\Delta i=-M\Delta u_{dc}\cos\Lambda-\Delta mU_{dc}\cos\Lambda \\ \qquad\qquad -U_s\Delta\varphi\sin\Phi \\ \Delta iL\omega=M\Delta u_{dc}\sin\Lambda+\Delta mU_{dc}\sin\Lambda+U_s\Delta\varphi\cos\Phi \\ C_d\dfrac{d\Delta u_{dc}}{dt}=\dfrac{1}{2}M\Delta i\cos\Lambda+\dfrac{1}{2}\Delta mI\cos\Lambda \end{cases} \tag{11}$$

Finally, the variation of the DC-link voltage for small changes of the converter current can be written in the Laplace domain using the following equation:

$$\frac{\partial u_{dc}}{\partial i}=\frac{-I\cos\Lambda\cos\Phi Ls+A\cos\Lambda}{2C_dU_{dc}\cos(\Lambda+\Phi)s+MI\cos\Lambda\cos(\Lambda+\Phi)} \tag{12}$$

where,

$$A=MU_{dc}\cos(\Lambda+\Phi)-IR_s\cos\Lambda-IL\omega\sin\Phi$$

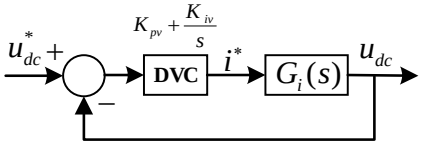

Fig.6 Block diagram of the simplified system model

The block diagram of the simplified system model is shown in Fig.6, in which a PI controller is used for the DVC, and $G_i(s)$ is the transfer function relating the amplitude of the converter current to the DC-link voltage as given by (12). The ACC is included in $G_i(s)$and can be represented for simplicity by a gain K_{pc}, representing a proportional controller.

Thus, the open loop transfer function becomes:

$$TF_{OL} = (K_{pv} + \frac{K_{iv}}{s})G_i(s) = (K_{pv} + \frac{K_{iv}}{s})\frac{\Delta u_{dc}}{\Delta i}K_{pc} = \frac{K_{pc}\cos\Lambda(Bs^2 + Cs + D)}{2C_d U_{dc}\cos(\Lambda+\Phi)s^2 + MI\cos\Lambda\cos(\Lambda+\Phi)s} \tag{13}$$

where,

$$B = -I\cos\Phi LK_{pv}$$
$$C = K_{pc}K_{pv}MU_{dc}\cos(\Lambda+\Phi) - K_{pc}K_{pv}IR_s\cos\Lambda - K_{pc}K_{pv}IL\omega\sin\Phi - K_{pc}K_{iv}I\cos\Phi L$$
$$D = K_{iv}\left[MU_{dc}\cos(\Lambda+\Phi) - IR_s\cos\Lambda - IL\omega\sin\Phi\right]$$

And then, the close loop transfer function can be derived as:

$$TF_{CL} = \frac{K_{pc}\cos\Lambda(Bs^2 + Cs + D)}{\left[2C_d U_{dc}\cos(\Lambda+\Psi) + BK_{pc}\cos\Lambda\right]s^2 + \left[MI\cos\Lambda\cos(\Lambda+\Psi) + CK_{pc}\cos\Lambda\right]s + DK_{pc}\cos\Lambda} \tag{14}$$

The initial values for the dynamic analysis can be calculated through the phasor diagram shown in Fig. 7, according to the load power and the theorem of conservation of power.

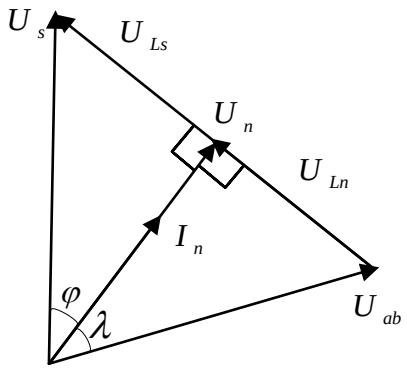

Fig.7 The phasor diagram of the simplified interaction system.

IV. Stability and Dynamic Performance Analysis for Different Operating Conditions

This section presents the dynamic performance and stability analysis of the train-network system using the small-signal model derived in section III using the system parameters reported in the Appendix.

A. Stability and dynamic performance analysis for different operating conditions

(1) The effect of the load power

Firstly, in order to check the dynamic performance of the train-network interaction for rated conditions, i.e. operating at rated power P=1200kW, and assuming the equivalent impedance of the traction power system is zero, the magnitude and phase diagrams of the transfer function (14) are shown in Fig.8 marked with circles. The curves illustrate that the controller is well designed for rated conditions, as it shows a fast system response and a satisfactory phase margin of 52 deg.

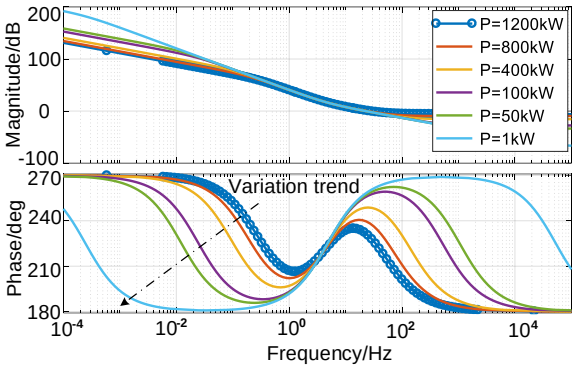

Fig.8 Bode plot for different load powers

The other curves in Fig. 8 show the effect of a reduced load power. From the analysis of the diagrams it can be concluded that when *P* decreases, the phase margin decreases significantly especially in low-frequency range, thus affecting both the dynamic performance and the stability of the system.

(2) The effect of presence of multiple trains

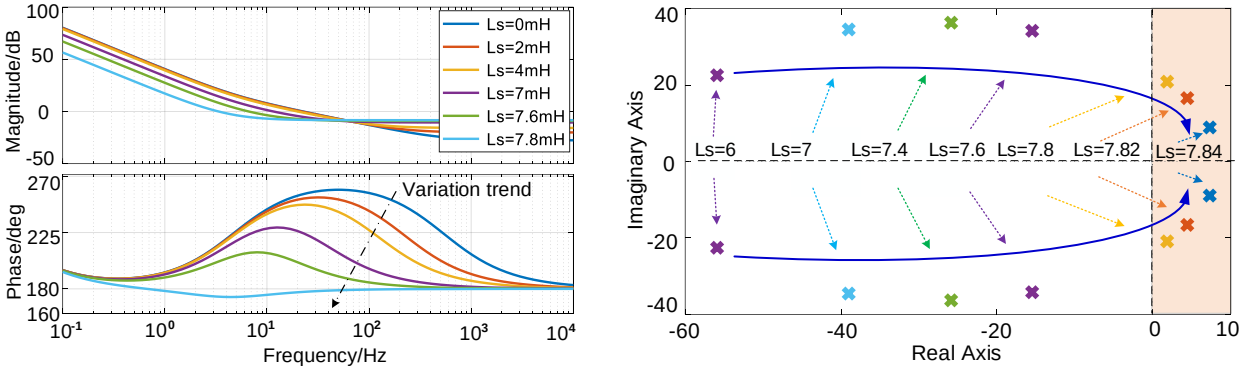

(a) Bode plot (b) Eigenvalue plot

Fig.9 Bode plot (a) and eigenvalue plot (b) for different inductance at the light-load condition (*P*=100kW).

Assuming that the converter is lightly loaded, the effect of the increase of the inductance L_s on the AC side of the converter, simulating the presence of multiple trains, are shown by the bode plots and eigenvalue plot in Fig. 9. From the Fig.9(a), the increase of L_s and, hence, the number of trains, causes a substantial decrease of the phase margin. Also, the phase in the frequency between 1 and 100 Hz reduces significantly, confirming the deterioration of the dynamic performance and stability.

Furthermore, as shown by the diagram in Fig.9(b), the eigenvalues move from the left half of the plane (LHP), indicating system stability, to the right half of the plane (RHP) , indicating instability. The critical value of the transition from LHP to RHP is about 7.78mH and approximately equal to 4 trains, which is in good agreement with the practical case.

B. Simulation analysis

In order to validate the theoretical analysis described above, the train-network system has been simulated in MATLAB/Simulink environment. With reference to a light-load condition of 100 kW, the waveforms of the line voltage, line current and DC-link voltage

are shown in Fig.10 with different inductance to simulate different number of trains simultaneously connecting to the railway power supply.

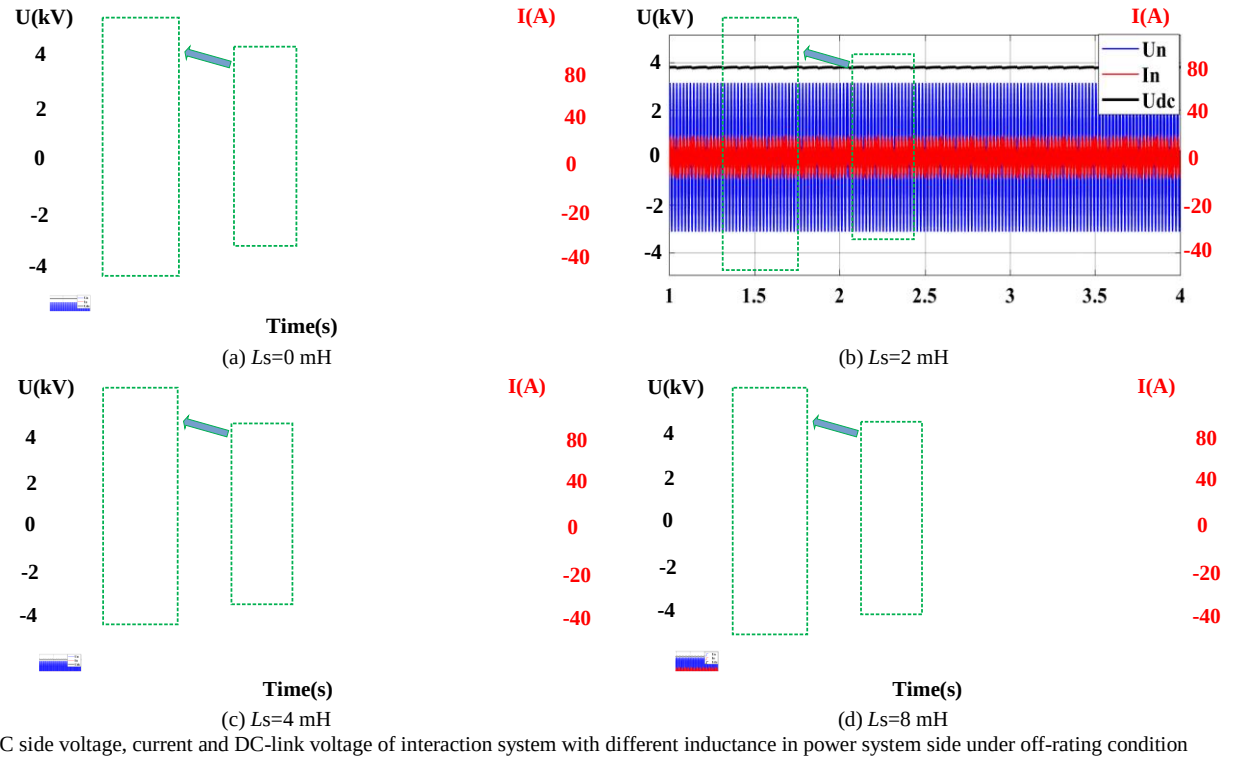

(a) *Ls*=0 mH (b) *Ls*=2 mH

(c) *Ls*=4 mH (d) *Ls*=8 mH

Fig.10The AC side voltage, current and DC-link voltage of interaction system with different inductance in power system side under off-rating condition

The results of the simulation show that with a larger inductance, the oscillations have larger magnitude and are quite evident when *Ls* is 8 mH (approximately equal to 4 trains). Simulations are in good agreement with the theoretical analysis and field measurement in terms of frequency and magnitude of the envelope of the AC voltage, AC current and the DC-link voltage.

C. Explanation of LFO occurrence

From the analysis above, it is evident that the possible cause of LFO is the mismatch between the controller parameters of the traction drive system and the actual characteristics of the train-network system. The schematic of the mismatch mechanism is shown in Fig. 11 and highlights that the controller tries to control a system that has different dynamic characteristics and stability from the designed ones.

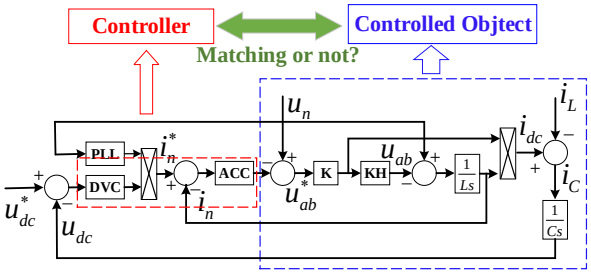

Fig.11The schematic diagram of the matching relation for the interaction system.

V. Tuning of the Controller Parameters and Adaptive Mitigation

According to the analysis in previous section, it is possible to investigate the effect of parameters tuning and design an adaptive

method to guarantee the matching of the interaction system, thus mitigating the problem of LFO.

A. The parameters tuning of DVC

The impact of parameters variation of DVC are outlined here. The dynamic performance for different proportional constants (*K*pv) are shown in Fig. 12(a). Although there is no substantial variation of the amplitude diagram, the rise of *K*pv noticeably enhances the phase margin especially in the low-frequency range between 0.1 Hz and 10 Hz, indicating an improvement of the dynamic performance and stability. The eigenvalue map in Fig.12(b) detailed explains that the eigenvalues move from RHP to LHP with tuning *K*pv from 0.05 to 0.25 and the critical value is about 0.18, which could be able to improve the stability and dynamic performance. Meanwhile, the simulations presented in Fig. 12(c) confirm that the growth of *K*pv stabilizes system's oscillation.

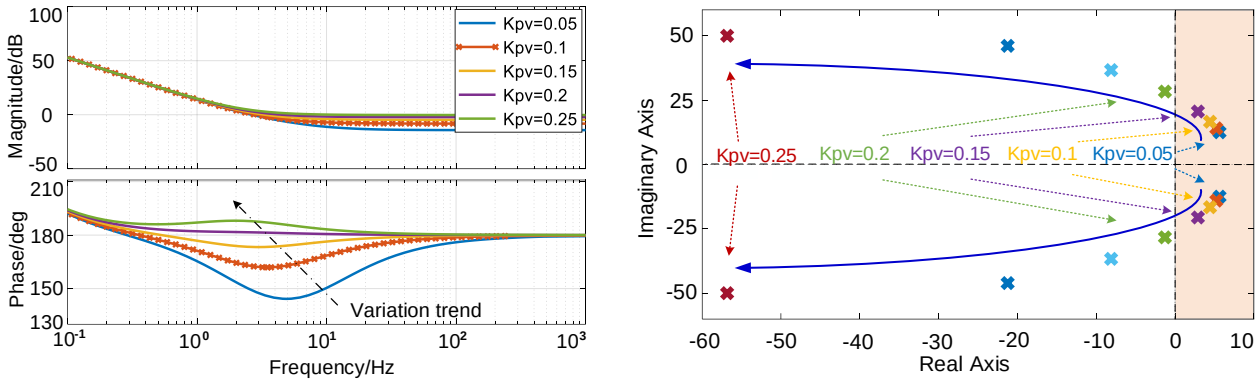

(a) Bode plot (b) Eigenvalue plot

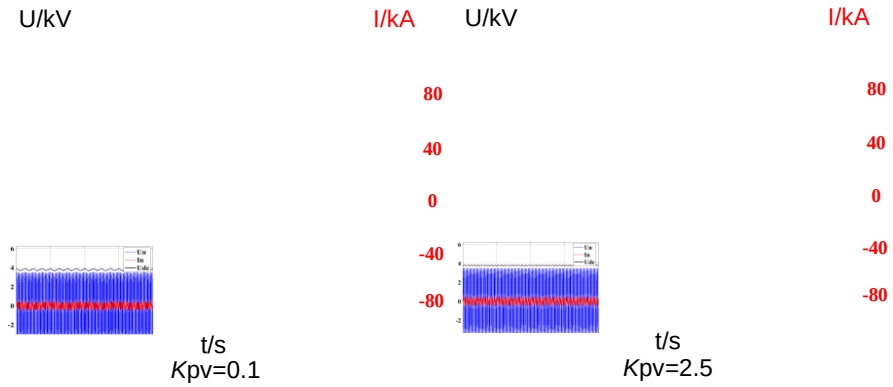

(c) Simulation results

Fig.12Response of the system with different proportional constants of DVC. Bode plot(a); Eigenvalue plot(b); Simulation results(c).

Furthermore, the effect of integral coefficient (*K*iv) is shown in Fig. 13. A decrease of *K*iv causes an climb of the phase margin in Fig.13(a) and, hence, an improvement of dynamic performance and stability. At the same time, Fig.13(b) shows that the eigenvalues move from RHP to LHP with the tuning of *K*iv from 4 to 0.5, and the critical value is about 1.5. Then, the simulation results in Fig. 13(c) confirm this as the oscillations become weaker.

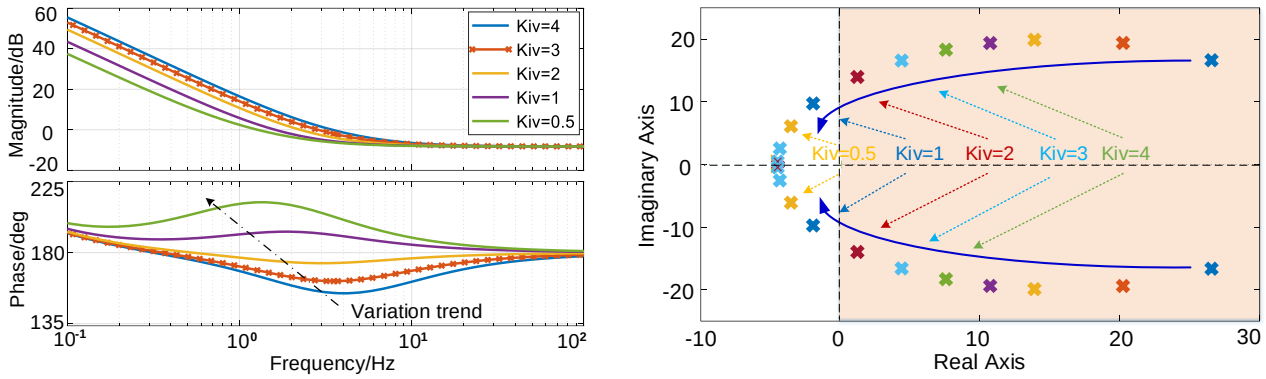

(a) Bode plot (b) Eigenvalue plot

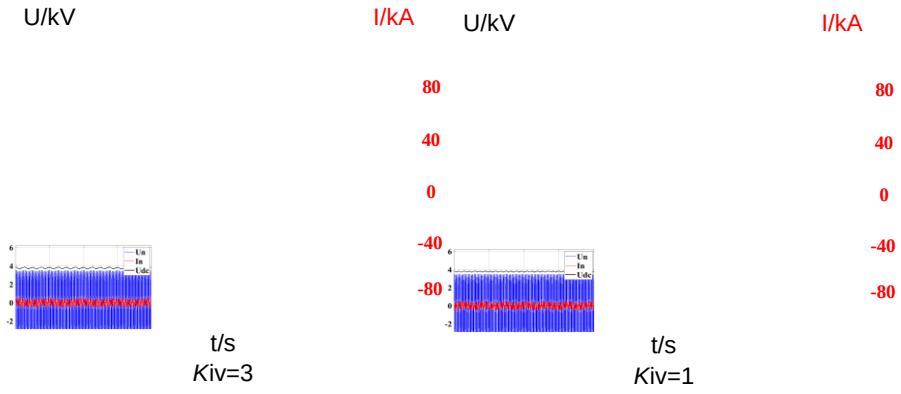

(c) Simulation results

Fig.13Response of the system for different integral constants of DVC. Bode plot(a); Eigenvalue plot(b); Simulation results(c).

B. The parameters tuning of ACC

Similarly, under this condition, the effect of the proportional constant (*K*pc) of ACC can be investigated. It can be found from bode diagram in Fig. 14(a) that with the rise of the *K*pc, the magnitude and phase both change, and the phase margin falls significantly. Fig.14(b) describes the eigenvalue movement from LHP to RHP as the increase of *K*pc from 0.01 to 2, and the critical value is about 0.02, indicating an deterioration of dynamic performance and stability. Then, the simulation results reveal the same features as shown in Fig. 14(c).

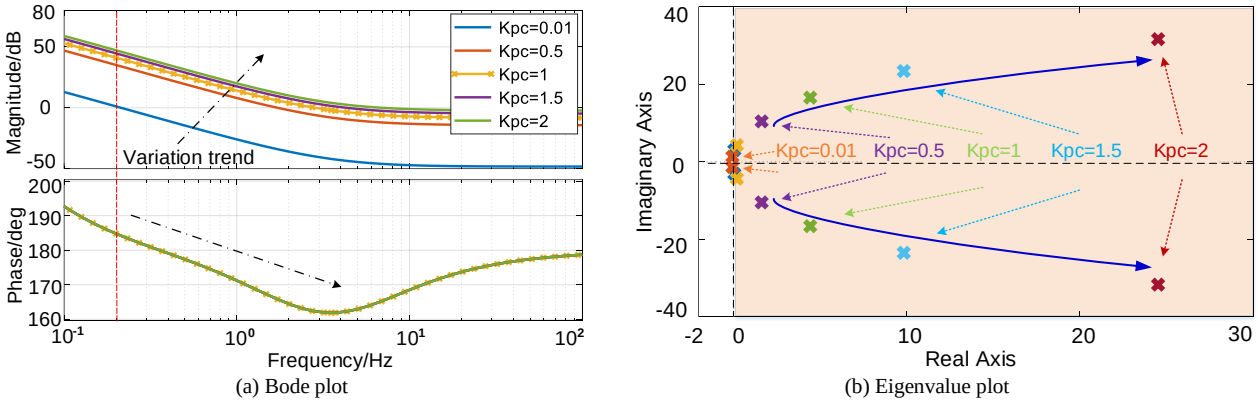

(a) Bode plot (b) Eigenvalue plot

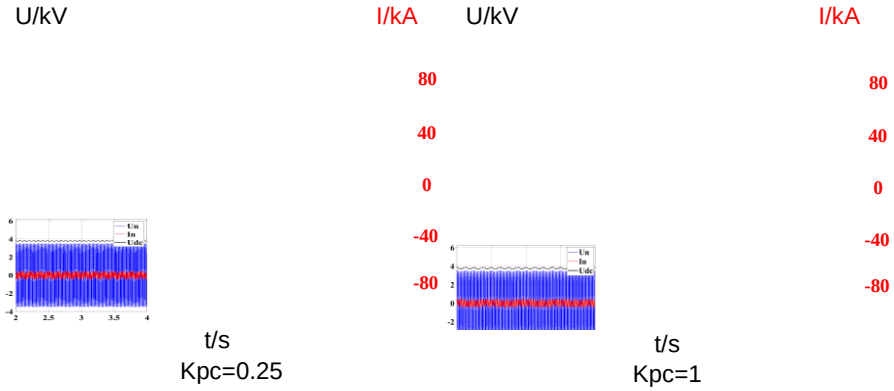

(c) Simulation results

Fig.14Response of the interaction system with different proportional constant (*K*pc) of ACC. Bode plot (a); Eigenvalue plot (b); Simulation results (c).

C. Experimental Verification

An experimental setup of the train-network system shown in Fig.15 is employed to verify the theoretical analysis in previous sub-section. The relevant parameters of the setup are listed in the Appendix.

According to the set of original parameters and rated load power, the train-network system can maintain normal operation. After the equivalent load shedding to simulate the light load working condition (off-rated power working condition), the reproduction of LFO is shown in Fig.16(a), which accords to the fact and the analysis in Section IV. Then selecting this working condition as the control group, the effects of the controller parameters are verified one by one. (1) With the growth of the *K*pv (from 0.1 to 3.5), the oscillations become weaker, as shown in Fig.16(b), which illustrates that the increase of *K*pv can improve the stability of the system; (2) If *K*iv continuously reduces from 0.2 to 0.01, the oscillations fall significantly, as shown in Fig. 16(c), so the decrease of *K*iv also can enhance stability; (3) As the decline of *K*pc (from 5 to 1), the system tends to be stable, as shown in Fig16(d). As a consequence, the experimental results show that the increase of *K*pv, the decrease of *K*iv and *K*pc all can lower the oscillation, whose variation tendency is consistent with the theoretical analysis, which can further provide the guidance for parameters tuning of the controller.

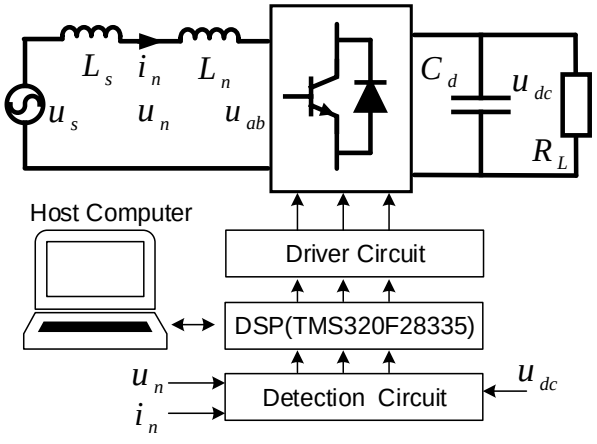

(a) System Structure

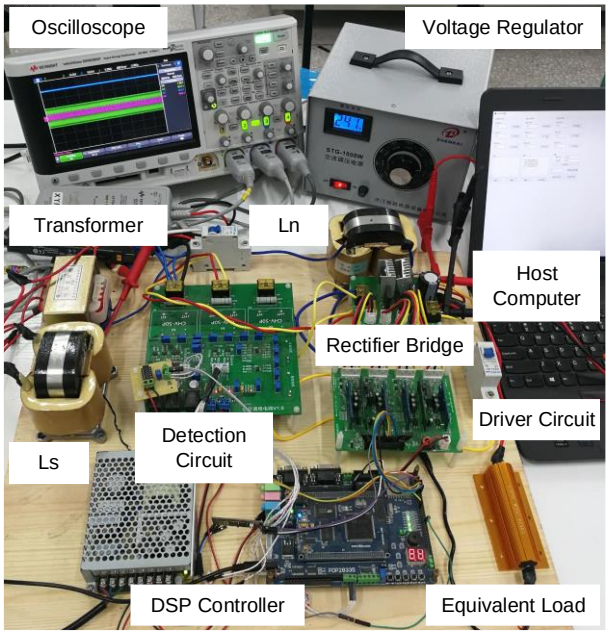

(b) Photo

Fig.15Experimental setup of train-network system. System structure (a); Photo (b).

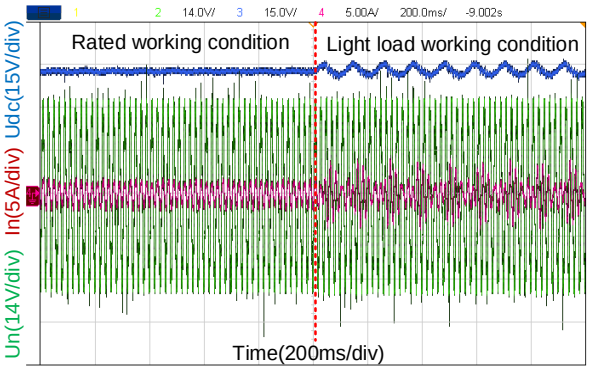

(a) The reproduction of the oscillation

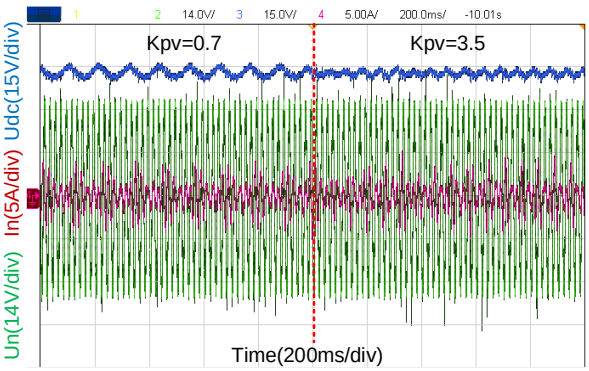

(b) The effect of *K*pv

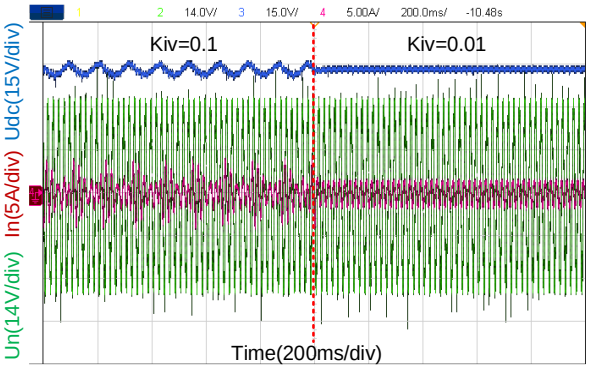

(c) The effect of *K*iv

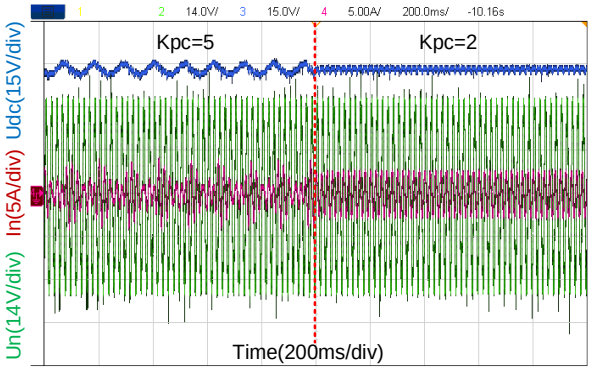

(d) The effect of *K*pc

Fig.16 Experimental verifications results. The effects of working condition (a), the parameters tuning *K*pv (b); *K*iv (c), *K*pc (d).

D. Adaptive mitigation and discussion

Summing up the above, the tuning of the controller parameters indeed can improve the dynamic performance and stability of the interaction system for the light-load working condition, which contributes to regaining the matching relation between the controller and the controlled object, and then can be further selected as an effective and economic suppression technique, and provides the tuning direction and tendency in order to mitigate the LFO in electrified railway. According to the background of actual controller design, the

train-network system should be able to keep up excellent dynamic performance and stability both for the rated working condition and the off-rated working condition. Therefore, it will be good if the controller should be able to select the different sets of parameters depending on the real-time load power. An adaptive mitigation method is proposed, whose flow diagram is shown in Fig.17.

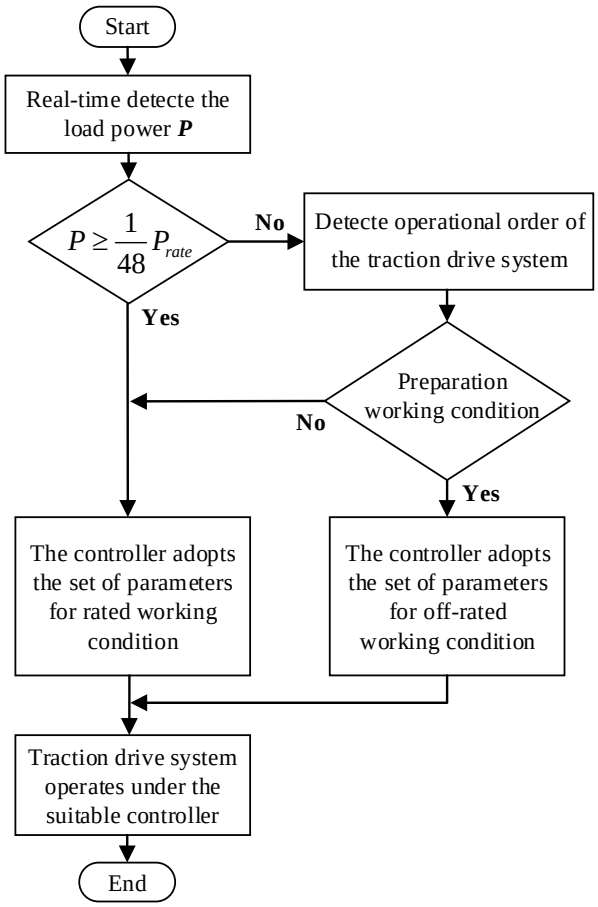

Fig.17The flow diagram of the adaptive tuning of controller for mitigating the LFO

The controller of the train-network system contains two sets of parameters: the one for rated working condition is the original parameter based on the current value, and the other one for off-rated working condition can be got with the help of the analysis in previous subsection, which could adaptively select the suitable parameters according to the actual load power. This adaptive tuning method of controller for mitigating the LFO comprises the following steps：

(1)Real-time detecting the load power, operational order and eliminating the interference of short-term mutation factors;

(2)If the load power $P \geqslant 1/48P_{rate}$(or the operational order of the locomotive is normal traction), the controller of the traction converter adopts the set of parameters for rated working condition;

(3)Otherwise, if the load power $P < 1/48P_{rate}$ and the operational order of the locomotive is preparation working condition, the controller of the traction converter adopts the set of parameters for off-rated working condition;

(4)The traction drive system operates under the control of the suitable controller parameters.

Then the effect of this adaptive method can be verified from the experimental setup. In the experiment, the original parameters for

the rated working condition follow the reference value (*K*pv=0.7, *K*iv=0.1 and *K*pc=5), and the tuned parameters for off-rated working condition adopt the values in previous subsection (*K*pv=3.5, *K*iv=0.01 and *K*pc=2). It can be observed that the LFO are mitigated using the tuned parameters under the condition of off-rated load power, and the whole process verification is shown in Fig.18.The results show that using an adaptive mitigation scheme to tune the parameters is effective to get rid of oscillations.

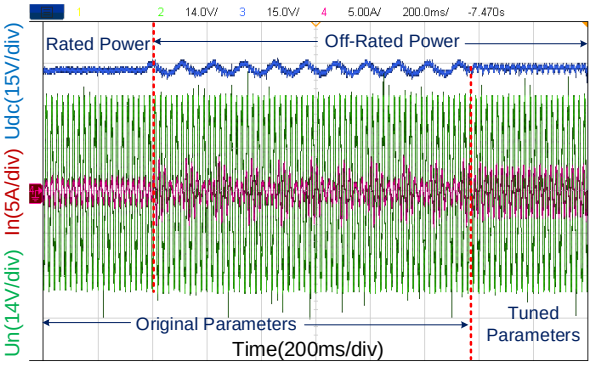

Fig.18The experimental verification of the adaptive mitigation method

Summing up the above, the adaptive method could greatly improve the LFO only with a small change to the existing train-network system. The control strategy and structure are same with the current one, so the engineering technicians are more likely to acquire this method. Thus, the further cooperation with the engineers from manufacturer of locomotive and Railway Bureau, in order to obtain more practical experience, will be the focus in the further work, which is significant to further guide the engineering mitigation of the LFO and has theoretical and practical meaning for the railway traffic.

VI. CONCLUSION

This paper introduces a mathematical model of the train-network system to reveal the generation mechanism of low-frequency oscillations caused by mismatching between the controller of the traction drive system and the actual controlled object. The proposed model taking into account the transient direct current control gives a clear and easy access to the evaluation of how working condition and control parameters variation may affect the stability and dynamic performance of interaction system. It has been shown that the changes of operating conditions are actually instrumental to the amplification of LFO and, when there are 4 or more trains connected to the catenary and drawing only limited power, there are serious risks of occurrence of the phenomenon. The tunings of the controller parameters show that the increase of *K*pv, the decrease of *K*iv and *K*pc all can reduce the oscillation and improve stability, whose results have been verified by simulations and experiments. Base on this, an adaptive mitigation scheme is developed, which can adaptively select the suitable parameters according to the actual load power in order to suppress the LFO. The proposed method can be implemented easily with minimal changes to the original system and thus improve the stability and dynamic performance of interaction system.

REFERENCE

[1] H. Hu, H. Tao, X. Wang, F. Blaabjerg, Z. He, and S. Gao, "Train-Network Interactions and Stability Evaluation in High-Speed Railways--Part II: Influential Factors and Verifications," *IEEE Transactions on Power Electronics*, vol. 33, pp. 4643--4659, 2018.

[2] H. Hu, Y. Shao, L. Tang, J. Ma, Z. He, and S. Gao, "Overview of harmonic and resonance in railway electrification systems," *IEEE Transactions on Industry Applications*, vol. 54, pp. 5227--5245, 2018.

[3] S. Danielsen, "Electric Traction Power System Stability: Low-frequency interaction between advanced rail vehicles and a rotary frequency converter,": Norwegian University of Science and Technology, 2010.

[4] H. Wang and M. Wu, "Review of low-frequency oscillation in electric railways," *Transactions of China Electrotechnical Society*, vol. 30, pp. 70--78, 2015.

[5] S. Danielsen, O. B. Fosso, M. Molinas, J. A. Suul, and T. Toftevaag, "Simplified models of a single-phase power electronic inverter for railway power system stability analysis—Development and evaluation," *Electric Power Systems Research*, vol. 80, pp. 204-214, 2010.

[6] C. Heising, M. Oettmeier, V. Staudt, and A. Steimel, "Improvement of low-frequency railway power system stability using an advanced multivariable control concept," in *Industrial Electronics, 2009. IECON'09. 35th Annual Conference of IEEE.*, 2009, pp. 560-565.

[7] X. Jiang, H. Hu, Z. He, H. Tao, and Q. Qian, "Study on low-frequency voltage fluctuation of traction power supply system introduced by multiple modern trains," *Electric Power Systems Research*, vol. 146, pp. 246-257, 2017.

[8] H. Wang, W. Mingli and J. Sun, "Analysis of Low-Frequency Oscillation in Electric Railways Based on Small-Signal Modeling of Vehicle-Grid System in dq Frame," *IEEE Transactions on Power Electronics*, vol. 30, pp. 5318-5330, 2015.

[9] J. Feng, W. Xu, Z. Chen, Z. Zhang, and W. Luo, "The Cause Analysis for Low-Frequency Oscillation of AC Electric Locomotive and Traction Power Supply Network," in *Proceedings of the 2015 International Conference on Electrical and Information Technologies for Rail Transportation*, 2016, pp. 597-608.

[10] J. Sun, "Small-signal methods for AC distributed power systems--a review," *IEEE Transactions on Power Electronics*, vol. 24, pp. 2545--2554, 2009.

[11] M. Amin and M. Molinas, "Small-Signal Stability Assessment of Power Electronics Based Power Systems: A Discussion of Impedance- and Eigenvalue-Based Methods," *IEEE Transactions on Industry Applications*, vol. 53, pp. 5014-5030, 2017.

[12] Y. Liao, Z. Liu, H. Zhang, and B. Wen, "Low-Frequency Stability Analysis of Single-phase System with dq-frame Impedance Approach – Part I: Impedance Modeling and Verification," *IEEE Transactions on Industry Applications*, p. 1-1, 2018.

[13] Z. Qionglin, "A Probe on Causes and Solutions of the HXD1 AC Locomotive's Resonance," *The World of Inverters*, vol. 5, pp. 40--44, 2009.

[14] C. G. H. Z. J Carter, "Analysis of the single-phase four-quadrant PWM converter resulting in steady-state and small-signal dynamic models," *IEE Proceedings-Electric Power Applications*, vol. 144, pp. 241-247, 1997.

[15] L. He, J. Xiong, H. Ouyang, P. Zhang, and K. Zhang, "High-performance indirect current control scheme for railway traction four-quadrant converters," *IEEE Transactions on Industrial Electronics*, vol. 61, pp. 6645--6654, 2014.

[16] M. Brenna, F. Foiadelli and D. Zaninelli, "New Stability Analysis for Tuning PI Controller of Power Converters in Railway Application," *IEEE Transactions on Industrial Electronics*, vol. 58, pp. 533-543, 2011.

[17] X. Jiang, H. Hu, J. Yang, Y. Zhou, Z. He, Q. Qian, P. Tricoli, S. Hillmansen, and C. Roberts, "The Mitigation Technology of Typical Low-Frequency Voltage Fluctuation in China Electrified Railway,": IEEE, 2018, pp. 632--637.

[18] F. Lin, Q. Lian, Z. Yang, J. Jiao, and Z. Zhang, "Analysis of low frequency voltage oscillation between AC drive electric locomotive and power supply networks," *Journal of the China Railway Society*, 2016.

[19] H. Hu, Y. Zhou, J. Yang, Z. He, and S. Gao, "A Practical Approach to Mitigate Low-Frequency Oscillation in Railway Electrification Systems," *IEEE Transactions on Power Electronics*, vol. 33, pp. 8198-8203, 2018.

[20] G. Zhang, Z. Liu, S. Yao, Y. Liao, and C. Xiang, "Suppression of low-frequency oscillation in traction network of high-speed railway based on auto-disturbance rejection control," *IEEE Transactions on Transportation Electrification*, vol. 2, pp. 244--255, 2016.

[21] Z. Liu, Z. Geng and X. Hu, "An Approach to Suppress Low Frequency Oscillation in the Traction Network of High-Speed Railway Using Passivity-Based Control," *IEEE Transactions on Power Systems*, vol. 33, pp. 3909-3918, 2018.

[22] C. Academy and R. Sciences, "Traction power supply test report of Datong-Qinhuangdao Railway HXD1 locomotive vehicle-network matching relationship," China Academy of Railway Sciences 2008.

[23] C. Academy and R. Sciences, "Catenary voltage and current test reports of Nanxiang opening and closing of CRH1067," 2010.

[24] C. Academy and R. Sciences, "Catenary voltage fluctuation test report of Xuzhou North Depot," 2011.

[25] S. Menth and M. Meyer, "Low frequency power oscillations in electric railway systems," *Elektrische Bahnen*, vol. 104, pp. 216 – 221, 2006.

[26] D. Lee and Y. Kim, "Control of single-phase-to-three-phase AC/DC/AC PWM converters for induction motor drives," *IEEE transactions on industrial electronics*, vol. 54, pp. 797--804, 2007.

[27] R. J. Hill, "Electric railway traction. II. Traction drives with three-phase induction motors," *Power Engineering Journal*, vol. 8, pp. 143--152, 1994.

[28] M. Brenna, F. Foiadelli and D. Zaninelli, "The Influence of Controller Parameters on the Quality of the Train Converter Current," *Advances in Power Electronics*, vol. 2011, pp. 1-10, 2011.

APPENDIX

Table II Circuit parameters of train-network system

Name	Symbol	Simulation Parameters	Experimental Parameters
AC-link voltage	U_S	2100 V	241 V
AC-link resistance	R_S	0Ω	0Ω
AC-link inductance	L_S	2mH	10mH

The ratio of transformer	k	25000/1450	220/18
DC-link voltage	U_{dc}	3775 V	42V
DC-link capacitance	C_d	3.9 mF	4.4 mF
Inductance of the converter	L_n	8 mH	10 mH
Reference frequency of power system	f_s	50 Hz	50 Hz
Proportional constants of voltage loop	K_{PV}	0.1	0.7
Integral constants of voltage loop	K_{IV}	3	0.1
Proportional constants of current loop	K_{PC}	1	5
Equivalent resistance of the load	R_L	370Ω	100Ω